THE JOURNAL OF BIOLOGICAL CHEMISTRY VOL. 285, NO. 46, pp. 36081–36091, November 12, 2010

Tyr-167/Trp-168 in Type 1/3 Inositol 1,4,5-Trisphosphate Receptor Mediates Functional Coupling between Ligand Binding and Channel Opening*[S]

Received for publication, May 1, 2010, and in revised form, August 1, 2010 Published, JBC Papers in Press, September 2, 2010, DOI 10.1074/jbc.M110.140129

Haruka Yamazaki[‡§], **Jenny Chan**[¶], **Mitsuhiko Ikura**[¶], **Takayuki Michikawa**[‡§1], **and Katsuhiko Mikoshiba**[‡§2]

From the [‡]*Laboratory for Developmental Neurobiology, RIKEN Brain Science Institute, Saitama 351-0198, Japan, the* [§]*Calcium Oscillation Project, Solution Oriented Research for Science and Technology, Japan Science and Technology Agency, Saitama 332-0012, Japan, and the* [¶]*Division of Signaling Biology, Ontario Cancer Institute and Department of Medical Biophysics, University of Toronto, Ontario M5G IL7, Canada*

The N-terminal ~220-amino acid region of the inositol 1,4,5-trisphosphate (IP_3) receptor (IP_3R)/Ca^{2+} release channel has been referred to as the suppressor/coupling domain because it is required for both IP_3 binding suppression and IP_3-induced channel gating. Measurements of IP_3-induced Ca^{2+} fluxes of mutagenized mouse type 1 IP_3R (IP_3R1) showed that the residues responsible for IP_3 binding suppression in this domain were not essential for channel opening. On the other hand, a single amino acid substitution of Tyr-167 to alanine completely impaired IP_3-induced Ca^{2+} release without reducing the IP_3 binding activity. The corresponding residue in type 3 IP_3R (IP_3R3), Trp-168, was also critical for channel opening. Limited trypsin digestion experiments showed that the trypsin sensitivities of the C-terminal gatekeeper domain differed markedly between the wild-type channel and the Tyr-167 mutant under the optimal conditions for channel opening. These results strongly suggest that the Tyr/Trp residue (Tyr-167 in IP_3R1 and Trp-168 in IP_3R3) is critical for the functional coupling between IP_3 binding and channel gating by maintaining the structural integrity of the C-terminal gatekeeper domain at least under activation gating.

The inositol 1,4,5-trisphosphate (IP_3)[3] receptor (IP_3R) functions as an IP_3-gated Ca^{2+} release channel localized on intracellular Ca^{2+} stores, such as the endoplasmic reticulum (1–3). IP_3R-mediated Ca^{2+} release occurs in complex spatial and temporal patterns, such as Ca^{2+} waves and Ca^{2+} oscillations, and Ca^{2+} regulates numerous cellular processes, including fertilization (4), cell proliferation (5), development (6, 7), secretion (8, 9), taste perception (10), synaptic plasticity (11–13), and growth cone navigation (14). In Ca^{2+} signaling cascades, IP_3R works as a signal converter that translates the information from IP_3 signals to Ca^{2+} signals (15). The mammalian IP_3R family consists of three isoforms (IP_3R1, IP_3R2, and IP_3R3) (16), which share 60–70% amino acid sequence identity (16, 17) and form homotetrameric or heterotetrameric channels (18). Because all three IP_3R isoforms show biphasic dependence on cytosolic Ca^{2+} with maximal Ca^{2+} releasing activities at submicromolar Ca^{2+} concentrations (19–21), Ca^{2+} has been proposed to work as a co-agonist of IP_3Rs (22).

The structure of IP_3R can be divided into three functional domains: an N-terminal IP_3-binding domain, a channel-forming domain localized to the C terminus, and a regulatory/coupling domain connecting these two domains (23, 24) (Fig. 1). The C-terminal channel-forming domain of IP_3R is further divided into two subdomains: a transmembrane domain and a gatekeeper domain (Fig. 1). The transmembrane domain contains six membrane-spanning regions (M1–M6) (25, 26), and an ion conduction pore has been proposed to be located in the hydrophobic segment between the M5 and M6 transmembrane regions (26–29) (Fig. 1). The cytosolic C-terminal tail region (residues 2590–2749) contains a cysteine residue, Cys-2613, that is critical for the activation gating, and this region has been proposed to work as a gatekeeper that triggers the opening of the activation gate of the channel following IP_3 binding (30).

The IP_3-binding domain is divided into two subdomains: an N-terminal suppressor domain and a C-terminal IP_3-binding core (Fig. 1). The IP_3-binding core is the minimum region required for specific IP_3 binding (31, 32) and consists of β-trefoil and α-helical fold domains (33). The IP_3-binding cores of all three isoforms show almost identical, high IP_3 binding affinities with equilibrium dissociation constants of ~2 nM (34). The N-terminal suppressor domain consists of a globular head subdomain forming a β-trefoil fold and an arm subdomain with a helix-turn-helix structure (35) and functions to attenuate the IP_3 binding affinity of the IP_3-binding core to generate isoform-specific IP_3 binding affinities (31, 34). Seven conserved residues clustered on one side of the head subdomain are critical for the IP_3 binding suppression (35), and 11 non-conserved residues in

* This work was supported by grants from the Special Postdoctoral Researchers Program in RIKEN (to H. Y.), Ministry of Education, Science, Sports, and Culture of Japan Grants 20370054 (to T. M.) and 20220007 (to K. M.), a Canadian Institutes of Health Research doctoral award (to J. C.), and a grant from the Heart and Stroke Foundation of Ontario (to M. I.).

[S] The on-line version of this article (available at http://www.jbc.org) contains supplemental Tables SI–SIV and Figs. S1–S9.

[1] To whom correspondence may be addressed: Laboratory for Developmental Neurobiology, RIKEN Brain Science Institute, 2-1 Hirosawa, Wako, Saitama 351-0198, Japan. Tel.: 81-48-467-9745; Fax: 81-48-467-9744; E-mail: t-michikawa@brain.riken.jp.

[2] To whom correspondence may be addressed: Laboratory for Developmental Neurobiology, RIKEN Brain Science Institute, 2-1 Hirosawa, Wako, Saitama 351-0198, Japan. Tel.: 81-48-467-9745; Fax: 81-48-467-9744; E-mail: mikosiba@brain.riken.jp.

[3] The abbreviations used are: IP_3, inositol 1,4,5-trisphosphate; IP_3R, IP_3 receptor; BCR, B-cell receptor; HEDTA, *N*-(2-hydroxyethyl)ethylenediaminetriacetic acid; βI, β-trefoil I; βII, β-trefoil II; α, Armadillo repeat-like α-helical fold.

the head subdomain are responsible for the generation of isoform-specific affinities (34). The N-terminal 223-amino acid region is required not only for suppression of IP_3 binding but also for channel gating because a mutant IP_3R1 lacking residues 1–223 did not exhibit any measurable IP_3-induced Ca^{2+} release activity, although it had 10-fold higher IP_3 binding affinity and seemed to retain the normal folded structure of the C-terminal channel-forming domain (30). Therefore, this N-terminal region is referred to as a suppressor/coupling domain and has been proposed to play a key role in connecting IP_3 binding with channel opening (30).

Limited trypsinization induces fragmentation of mouse IP_3R1 into five major fragments (Fig. 1), and the four N-terminal cytosolic fragments (I, II, III, and IV) are associated with the remaining C-terminal fragment V that encompasses the channel-forming domain (36, 37). Trypsinized IP_3R retains significant IP_3-induced Ca^{2+} release activity (37), indicating that structural coupling among the five split components allows functional coupling between IP_3 binding and channel opening. Expression of the channel-forming domain of mouse IP_3R1 (residues 2216–2749) alone increases Ca^{2+} leakage from the endoplasmic reticulum in intact cells (38), suggesting that the channel-forming domain forms a constitutively active channel and that the N-terminal cytosolic region (residues 1–2215) is necessary to keep the channel domain closed. Cross-linking experiments of trypsin-digested IP_3R showed that the N-terminal tryptic fragment I (~340 residues) containing the suppressor/coupling domain and part of the IP_3-binding core is located near the C-terminal tryptic fragment V (39). Because deletion of the M4-M5 linker, comprising the cytosolic region between transmembrane regions M4 and M5 (Fig. 1), facilitates the dissociation of fragment I from trypsin-treated microsomal vesicles and disrupts the IP_3-induced Ca^{2+} flux in COS-7 cells, Schug and Joseph (40) have proposed that one C-terminal site for the interaction between the N-terminal IP_3-binding site and the C-terminal channel-forming domain is within the M4-M5 linker and that IP_3-induced conformational changes in the N-terminal IP_3-binding domain are mechanically transmitted to pore opening through an attachment to the M4-M5 linker. However, the residues that directly interact with the M4-M5 linker have not been identified.

In this study, we searched for critical residues for channel gating within the N-terminal suppressor/coupling domain and found that a single amino acid substitution at Tyr-167 completely disrupted the IP_3-induced Ca^{2+} release activity of IP_3R1. The corresponding residue in IP_3R3, Trp-168, was also required for channel opening. Biochemical analyses in this study and an accompanying paper (57) produced strong evidence that these residues directly interacted with the M4-M5 linker within the C-terminal channel-forming domain. Quantitative measurements of the digestion rate of the C-terminal gatekeeper domain after trypsin digestion suggested that the Tyr/Trp residue (Tyr-167 in IP_3R1 and Trp-168 in IP_3R3) within the suppressor/coupling domain acts to maintain the structural integrity of the gatekeeper domain.

EXPERIMENTAL PROCEDURES

Plasmid Construction—The details of these procedures are given in the supplemental material.

Generation of Stable Cell Lines and Microsome Preparation—Stable cell lines expressing recombinant IP_3Rs were established from intrinsically IP_3R-deficient R23-11 cells (41) as described previously (30). Microsomal fractions were prepared as described previously (30, 42) and suspended in cytosol-like medium (110 mM KCl, 10 mM NaCl, 5 mM KH_2PO_4, 1 mM DTT, 50 mM HEPES-KOH, pH 7.2, at room temperature) that was passed through Chelex-100 (Bio-Rad) and supplemented with protease inhibitors. Protein concentrations were determined with a protein assay kit (Bio-Rad) using BSA as a standard.

IP_3 Binding Assay—The IP_3 binding affinity of IP_3R was measured as described previously (17, 43). Microsomal fractions (30 μg) in cytosol-like medium (pH 7.4 at 4 °C) containing 0.5 mM EGTA were incubated with 0.15–11 nM [^{3}H]IP_3 (PerkinElmer Life Sciences) and various concentrations (10–400 nM) of unlabeled IP_3 (Dojindo). Nonspecific binding was measured in the presence of 10 μM unlabeled IP_3. Nonlinear regression of the IP_3 binding data was performed with the Hill-Langmuir equation,

$$B = B_{max}\frac{[IP_3]}{K_d + [IP_3]} \quad \text{(Eq. 1)}$$

where B is the concentration of IP_3 bound to the receptor, B_{max} is the concentration of the total binding sites, $[IP_3]$ is the free IP_3 concentration, and K_d is the dissociation constant.

Quantification of IP_3-induced Ca^{2+} Release Activity of Mutant IP_3R Channels—The IP_3-induced Ca^{2+} efflux from microsomal vesicles was monitored using a method described previously (37) with modifications. Briefly, microsomal fractions (300 μg of protein) were suspended in 500 μl of cytosol-like medium that was passed through Chelex-100 and supplemented with 1 μg/ml oligomycin (Sigma), 2 mM $MgCl_2$, 25 μg/ml creatine kinase (Roche Applied Science), 10 mM phosphocreatine (Sigma), and 2 μM fura-2 (Dojindo). The suspension was stirred continuously at 30 °C during measurements. Ca^{2+} was accumulated within microsomal vesicles by the addition of 1 mM ATP after the addition of an aliquot (≤3 μl) of 0.5 mM $CaCl_2$. IP_3 was applied when the concentration of extravesicular free Ca^{2+} was within the range of 400–500 nM. The total amount of releasable Ca^{2+} within the vesicles was measured by the addition of 2 μM Ca^{2+} ionophore 4-BrA23187 (Sigma). Fluorescent signals of fura-2 were monitored at 20 Hz with a CAF-110 spectrofluorometer (Jasco) and a PowerLab data acquisition system (ADInstruments). An emission wavelength of 510 nm with alternate excitation at 340 and 380 nm (F340 and F380, respectively) was used. For calibration of the fura-2 signals, 1 mM $CaCl_2$ and 10 mM EGTA were sequentially added at the end of each measurement. The Ca^{2+} concentrations were calculated as described previously (44).

Limited Trypsin Digestion—Limited trypsin digestion was performed as described previously (37) with modifications. Briefly, microsomal vesicles (2 mg of protein/ml) were incu-

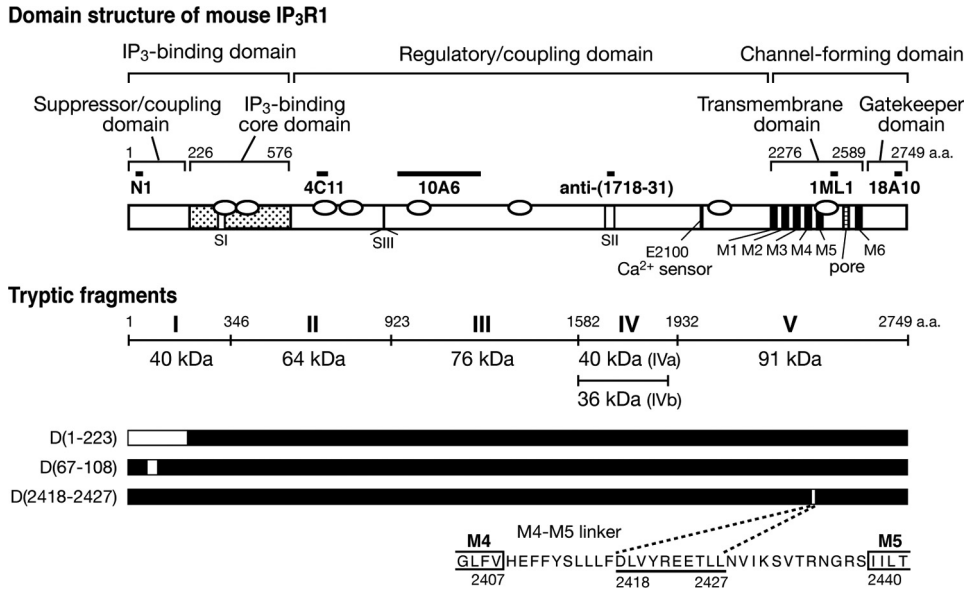

FIGURE 1. **Domain structures of mouse IP_3R1 and the deletion mutants used in this study.** A *schematic diagram* of the primary structure of mouse IP_3R1 (*SI+*, *SII+*, *SIII−*) (NCBI accession number X15373) is shown. The *dotted box* represents the IP_3-binding core domain (residues 226–576). The *black boxes* (M1, M2, M3, M4, M5, and M6) represent membrane-spanning regions, and the *striped box* represents a channel pore. *SI*, *SII*, and *SIII* represent the regions spliced out in alternative splicing variants. Putative Ca^{2+} binding sites (53, 54) are indicated by *open ovals*. The regions containing the epitopes for the N1, 4C11, 10A6, anti-(1718-31), 1ML1, and 18A10 antibodies are indicated by *thick horizontal lines*. The molecular masses of the major tryptic fragments (*I–V*) are indicated. The glutamate residue proposed to be a Ca^{2+} sensor (52) is shown (*E2100*). The amino acid sequence around the deleted segment in D(2418–2427) and boundaries of transmembrane regions M4 and M5 (55) are also shown.

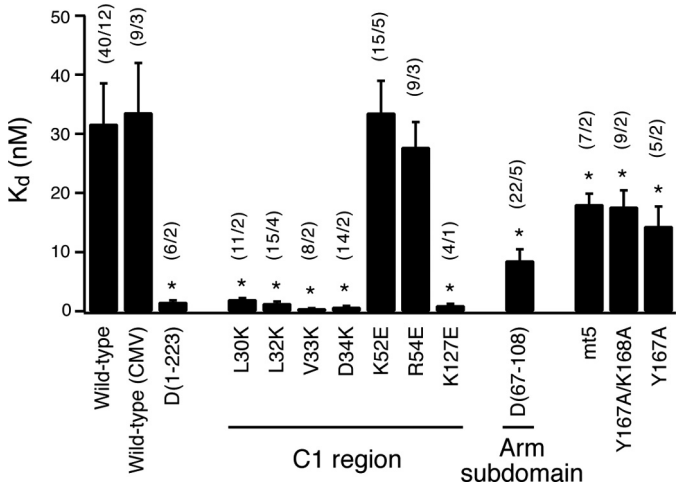

FIGURE 2. **IP_3 binding affinities of the mutant IP_3R1 channels.** The IP_3 dissociation constants of wild-type IP_3R1 and various mutants are shown. All of the IP_3R1 channels were expressed with the β-actin promoter, except for wild type (*CMV*), which was expressed with the CMV promoter. *Error bars*, S.D. The numbers of measurements (n_1) and numbers of cell lines used (n_2) are shown in *parentheses* as (n_1/n_2). *, $p < 0.01$ *versus* the value of wild-type IP_3R1 expressed with the β-actin promoter by Scheffé's F-test.

bated with 2 μg/ml *N*-tosyl-L-phenylalanyl chloromethyl ketone-treated trypsin (Sigma) at 35 °C in a buffer comprising 110 mM KCl, 10 mM NaCl, 1 mM EGTA, 1 mM DTT, and 50 mM HEPES-KOH (pH 7.33 at 35 °C). The free Ca^{2+} concentrations in the buffer were adjusted using HEDTA and confirmed with a Ca^{2+}-sensitive electrode (Metrohm) as described previously (42). The apparent dissociation constant of HEDTA for Ca^{2+} in the buffer was estimated to be 2.64 μM. The trypsin digestion was terminated by the addition of 100 μg/ml soybean trypsin inhibitor (Sigma) and 0.1 mM phenylmethylsulfonyl fluoride (Sigma). After the trypsin treatment, the microsomal lysates were centrifuged at 20,000 × *g* for 30 min. The supernatants were concentrated by 4-fold by 10% trichloroacetic acid precipitation. Trypsin-treated microsomal lysates (14.6 μg of protein/lane) and supernatants obtained from 58.5 μg of microsomal protein/lane were applied to 7.5% SDS-PAGE. Tryptic fragments of recombinant IP_3R1 were detected by Western blotting using N1, 4C11, 10A6, anti-(1718-31), 18A10, and 1ML1 antibodies (Fig. 1) (37) and quantified using the ImageJ software (National Institutes of Health). To calculate the ratios of the intensities of the 18A10 signals and the 1ML1 signals, we applied all of the samples obtained from single experiments onto single SDS-polyacrylamide gels, and both the 18A10 and 1ML1 signals were collected from the same membrane by stripping and reprobing.

RESULTS

Ca^{2+} Release Activities of Mutant IP_3R1 Channels in Which Residues Critical for IP_3 Binding Suppression Are Altered—In a previous study (35), we identified a set of amino acid residues (Leu-30, Leu-32, Val-33, Asp-34, Arg-36, Arg-54, and Lys-127) that comprise a critical site for IP_3 binding suppression in the context of an N-terminal 604-amino acid construct of mouse IP_3R1 ($T604_{m1}$). To investigate whether these residues are required for channel gating, we constructed nine different full-length IP_3R1 constructs that encoded eight single point mutants (L30K, L32K, V33K, D34K, R36E, K52E, R54E, and K127E) and one deletion mutant, D(67–108), lacking the arm subdomain (Fig. 1). We introduced these IP_3R1 mutant constructs into intrinsically IP_3R-deficient R23-11 cells derived from chicken B-cell line DT40 cells (41) and attempted to establish cell lines stably expressing each of the recombinant proteins using a method described previously (30). We successfully obtained cell lines for eight of the mutants but could not establish stable cell lines expressing R36E under the conditions used. Because the expression levels of the recombinant proteins varied from cell line to cell line (see below), multiple cell lines were used for the following assays.

In equilibrium [^{3}H]IP_3 binding analyses, five mutants (L30K, L32K, V33K, D34K, and K127E) exhibited significantly high IP_3 binding affinities (Fig. 2 and supplemental Table SIII) that were comparable with that of D(1–223) lacking the entire suppressor/coupling domain (Fig. 1) (30), thereby confirming that these residues are critical for IP_3 binding suppression within the

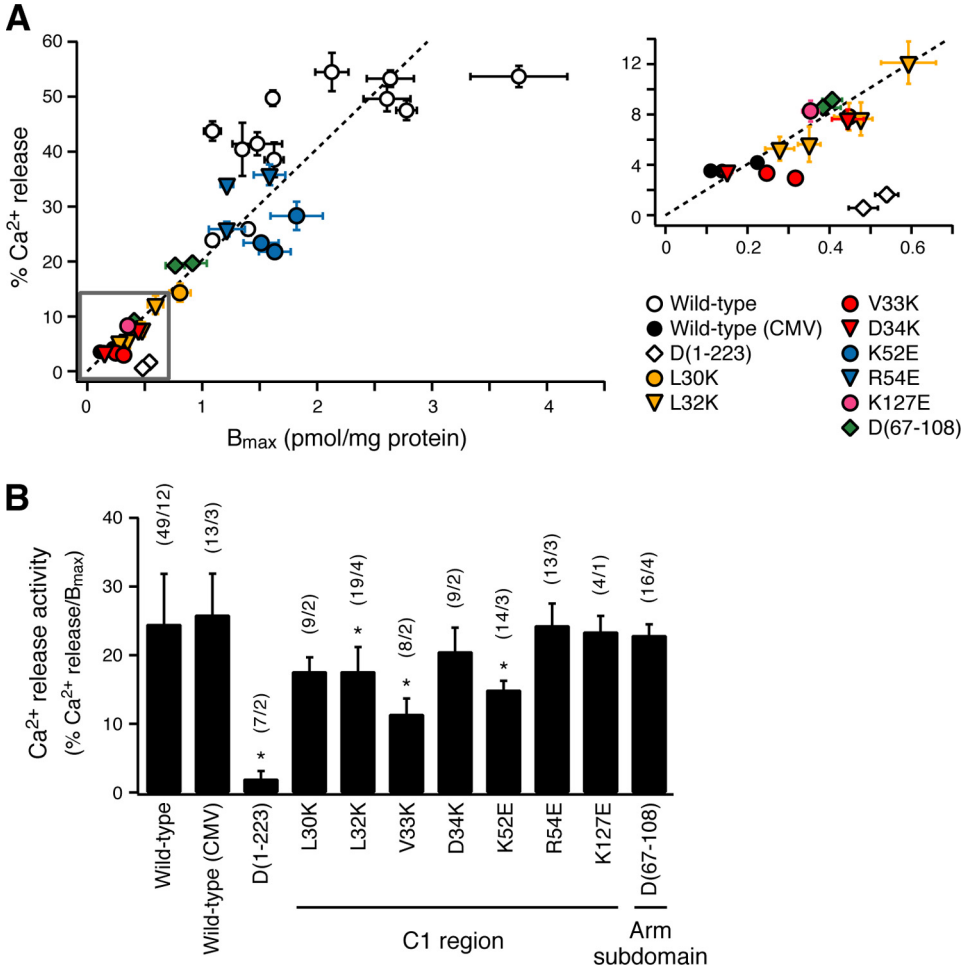

FIGURE 3. **Ca^{2+} release activities of the mutant IP_3R1 channels.** *A*, relationship between the expression levels of recombinant IP_3R1 channels and the fractions of Ca^{2+} released from microsomal vesicles by the addition of 1 μM IP_3. The expression levels of the channels are shown as the number of IP_3-binding sites per 1 mg of microsomal protein (B_{max}). The results for each cell line are plotted separately ($n \geq 4$ for the percentage of Ca^{2+} release and $n \geq 3$ for B_{max}). *Error bars*, S.D. The *broken line* indicates the relationship between the expression level and the fraction of Ca^{2+} release of wild-type IP_3R1. The portion enclosed in the *gray square* is shown in the *inset*. *B*, the fraction of Ca^{2+} release was divided by the expression level of the receptor (% Ca^{2+} *release*/B_{max}), and the means of all of the data obtained for each mutant are shown. *Error bars*, S.D. The numbers of measurements (n_1) and numbers of cell lines used (n_2) are shown in *parentheses* as (n_1/n_2). *, $p < 0.01$ *versus* the value of wild-type IP_3R1 expressed with the β-actin promoter by Scheffé's F-test.

(supplemental Fig. S1*A*). Because the fraction of Ca^{2+} released by IP_3 relative to the total amount of releasable Ca^{2+} in the vesicles was relatively constant regardless of the amount of releasable Ca^{2+} (supplemental Fig. S1*B*), we used the fractional values as percentages to estimate the IP_3-induced Ca^{2+} release activities of the mutant channels. Fig. 3*A* shows the relationship between the fractions of IP_3-induced Ca^{2+} release and the expression levels of the wild-type and mutant IP_3R1 channels. Because the expression levels of most of the mutants were lower than that of wild-type IP_3R1 (Fig. 3*A*), even when the same chicken β-actin promoter was used to establish the cell lines, we also used the CMV promoter to obtain cell lines expressing lower amounts of wild-type IP_3R1. The amount of Ca^{2+} release by the wild-type channel was proportional to its expression level with a slope of 20.3%/(pmol/mg protein) (R^2 = 0.631) (Fig. 3*A*). Similar responses were observed for all of the mutants except for the non-functional D(1–223) mutant. To compare the Ca^{2+} release activities between the wild-type and mutant channels directly, we calculated the percentage of Ca^{2+} release per unit amount of each channel expressed. The L32K, V33K, and K52E mutants exhibited Ca^{2+} release activities that were lower than that of wild-type IP_3R1 but significantly higher than that of the D(1–223) mutant (Fig. 3*B*). The L30K, D34K, R54E, K127E, and D(67–108) mutants exhibited Ca^{2+} release activities that were indistinguishable from that of wild-type IP_3R1 (Fig. 3*B*). These results suggest that the residues responsible for modulating the IP_3 binding affinity and the arm subdomain in the suppressor/coupling domain are not directly involved in the functional communication with the channel-forming domain of the receptor.

tetrameric channel complex. On the other hand, R54E, which is less effective in liberating the effect of the suppressor domain on IP_3 binding to $T604_{m1}$ (35), exhibited no change in the binding affinity compared with that of wild-type IP_3R1 (Fig. 2 and supplemental Table SIII). Similarly, the K52E mutant, which induces a significant decrease in the IP_3 binding affinity of $T604_{m1}$ (35), showed no effect on IP_3 binding in the context of full-length IP_3R1 (Fig. 2 and supplemental Table SIII). Finally, the D(67–108) construct lacking the arm subdomain showed a significant increase in the IP_3 binding affinity compared with the full-length IP_3R1 construct (Fig. 2 and supplemental Table SIII), similar to that observed for $T604_{m1}$ (35). Taken together, these results for the full-length IP_3R1 constructs are highly consistent with the findings of a previous mutagenesis study using $T604_{m1}$ constructs (35).

To examine the IP_3-induced Ca^{2+} release activities of the mutants, we monitored 1 μM IP_3-induced Ca^{2+} fluxes from microsomal vesicles prepared from the stable cell lines

Identification of the Residue Responsible for IP_3-induced Channel Gating within the Suppressor/Coupling Domain—We hypothesized that the critical residues for channel gating should be highly conserved amino acid residues that are localized on the molecular surface of the suppressor/coupling domain (Fig. 4*A*, *top*). According to this hypothesis, we selected 26 amino acid residues for evaluation (Fig. 4*A*, *bottom*). Five amino acid residues (Asp-35, Pro-49, Pro-50, Lys-51, and Phe-53) within the most conserved surface region (C1) (35) were singly or doubly substituted in mutant constructs (D35K,

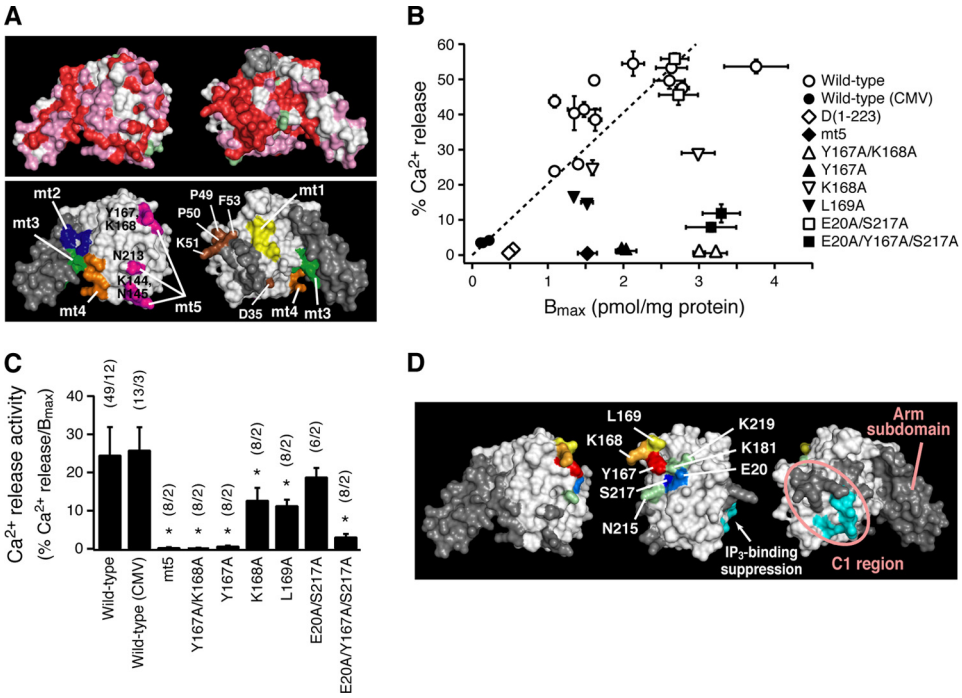

FIGURE 4. **Identification of the critical residue for the IP_3-induced channel gating of IP_3R1.** *A*, surface representations of the N-terminal 223 amino acid residues of IP_3R1 (Protein Data Bank accession number 1XZZ). The surface residue conservation determined from sequence alignments of mouse IP_3R1, IP_3R2, and IP_3R3 (NCBI accession numbers X15373, AB182288, and AB182289, respectively); *Xenopus laevis* IP_3R1 (D14400); and IP_3Rs cloned from *Drosophila melanogaster* (D90403), *Panulirus argus* (AF055079), *Asterina pectinifera* (AB071372), and *Caenorhabditis elegans* (AJ243179) is plotted using the following *color code*: *red*, 100% identity; *pink*, 70–90% identity; *white*, 30–70% identity; *pale green*, 0–30% identity. The C-terminal tag, Leu-Glu-His-His-His, is shown in *gray*. In the *lower panel*, the residues substituted to alanine are shown in *yellow* (mt1; Ile-14, Lys-59, Leu-126, and Asn-129), *blue* (mt2; Met-63, Arg-65, and Trp-160), *green* (mt3; Tyr-66, Gln-69, Trp-73, Asn-156, and Glu-157), *orange* (mt4; Lys-136, Arg-137, Ser-159, and Asn-188), and *magenta* (mt5; Lys-144, Asn-145, Tyr-167, Lys-168, and Asn-213), whereas the residues substituted or deleted in the mutants shown in Fig. 3 are *colored* in *gray*. The views on the *left* were rotated by 210° relative to the views on the *right*. *B*, relationship between the expression levels of recombinant IP_3R1 channels and the fractions of Ca^{2+} released from microsomal vesicles ($n \geq 3$ for percentage of Ca^{2+} release and $n \geq 3$ for B_{max}) by the addition of 1 μM IP_3. The *broken line* indicates the relationship between the expression level and the fraction of Ca^{2+} release mediated by the wild-type channel. *Error bars*, S.D. *C*, Ca^{2+} release activities of the mutant channels. *Error bars*, S.D. The numbers of measurements (n_1) and numbers of cell lines used (n_2) are shown in parentheses as (n_1/n_2). *, $p < 0.01$ *versus* the value of wild-type IP_3R1 expressed with the β-actin promoter by Scheffé's F-test. *D*, surface representations of Tyr-167 and the 7 surrounding residues evaluated. The 6 residues critical for IP_3 binding suppression, namely Leu-30, Leu-32, Val-33, Asp-34, Arg-36, and Lys-127 (35), are shown in *cyan*. All of the residues analyzed in this study except the above 14 residues are *colored* in *gray*. *Left*, view of the *middle image* rotated by −90°. *Right*, view of the *middle image* rotated by 90°.

P49A/P50D, K51E, and F53D) (Fig. 4*A*, *bottom*). The remaining 21 residues were divided into five groups, mt1 (*yellow*), mt2 (*blue*), mt3 (*green*), mt4 (*orange*), and mt5 (*magenta*) (Fig. 4*A*, *bottom*), and five mutant IP_3R1 cDNAs in which all of the residues in each group were substituted to alanine were constructed. The Ca^{2+} release activities of the mutant channels were examined by measuring the B-cell receptor (BCR)-induced cytosolic Ca^{2+} increases (supplemental Fig. S2, *A* and *B*) in mutant IP_3R-expressing cells established from R23-11 cells. We found that the Ca^{2+} increases were largely impaired in mt5-expressing cells (supplemental Fig. S2, *A* and *B*) despite sufficient amounts of protein expression (supplemental Fig. S2*C*). Thapsigargin-induced Ca^{2+} increases were observed in the mt5-expressing cells (supplemental Fig. S2, *A* and *B*), suggesting that the Ca^{2+} stores were intact. The mt5 mutant bound to IP_3 with a K_d value of 18 ± 2 nM (Fig. 2 and supplemental Table SIII). These results suggest that the critical residues for channel gating are present in the five residues selected for mt5.

To identify the specific residues critical for channel gating, we made three mutants (K144A/N145A, N213A, and Y167A/K168A) of full-length mouse IP_3R1. Among these mutants, only the Y167A/K168A mutant significantly reduced the amplitude of the BCR-induced Ca^{2+} increases (supplemental Fig. S2*B*). To determine whether both Tyr-167 and Lys-168 are required for channel gating, we made two additional mutants (Y167A and K168A) of mouse IP_3R1. As shown in supplemental Fig. S2*B*, the BCR-induced Ca^{2+} increases were almost intact in the cells expressing the Y167A or K168A mutant. However, by measuring the IP_3-induced Ca^{2+} release from isolated microsomal vesicles, we found that in addition to mt5 and Y167A/K168A, the Y167A mutant almost completely lost the IP_3-induced Ca^{2+} release activity, whereas the K168A mutant retained ~50% of the activity (Fig. 4, *B* and *C*). Y167A bound to IP_3 with a K_d value of 14 ± 3 nM (Fig. 2 and supplemental Table SIII). Trypsin digestion of the Y167A/K168A mutant generated the same tryptic fragments as wild-type IP_3R1 (supplemental Fig. S3), indicating that the mutations at either Tyr-167 or Lys-168 did not influence the global structure of IP_3R1. Because the rate of ATP-induced Ca^{2+} accumulation into microsomal vesicles prepared from the Y167A-expressing cells was comparable with the rate of Ca^{2+} accumulation into microsomal vesicles prepared from wild-type IP_3R1-expressing cells (supplemental Fig. S4), the mutant did not seem to form leaky Ca^{2+} channels. On the basis of these results, we concluded that Tyr-167 of IP_3R1 is a critical residue for IP_3-induced channel opening and that Lys-168 plays a supporting role for the gating process.

Fig. 4*D* shows a surface representation of Tyr-167 within the suppressor/coupling domain. Tyr-167 is located on the reverse side of the C1 region (Fig. 4*D*). We analyzed whether other residues near Tyr-167, such as Leu-169, Lys-181, Asn-215, and Lys-219 (Fig. 4*D*), are involved in the gating process triggered by IP_3 binding. We found a remarkable decrease in the fraction of IP_3-induced Ca^{2+} release from microsomal vesicles isolated from L169A-expressing cells (supplemental Fig. S5). This single amino acid substitution at Leu-169 resulted in a 54% reduction in the Ca^{2+} release activity (Fig. 4, *B* and *C*). These results suggest that Leu-169 is also involved in the gating process.

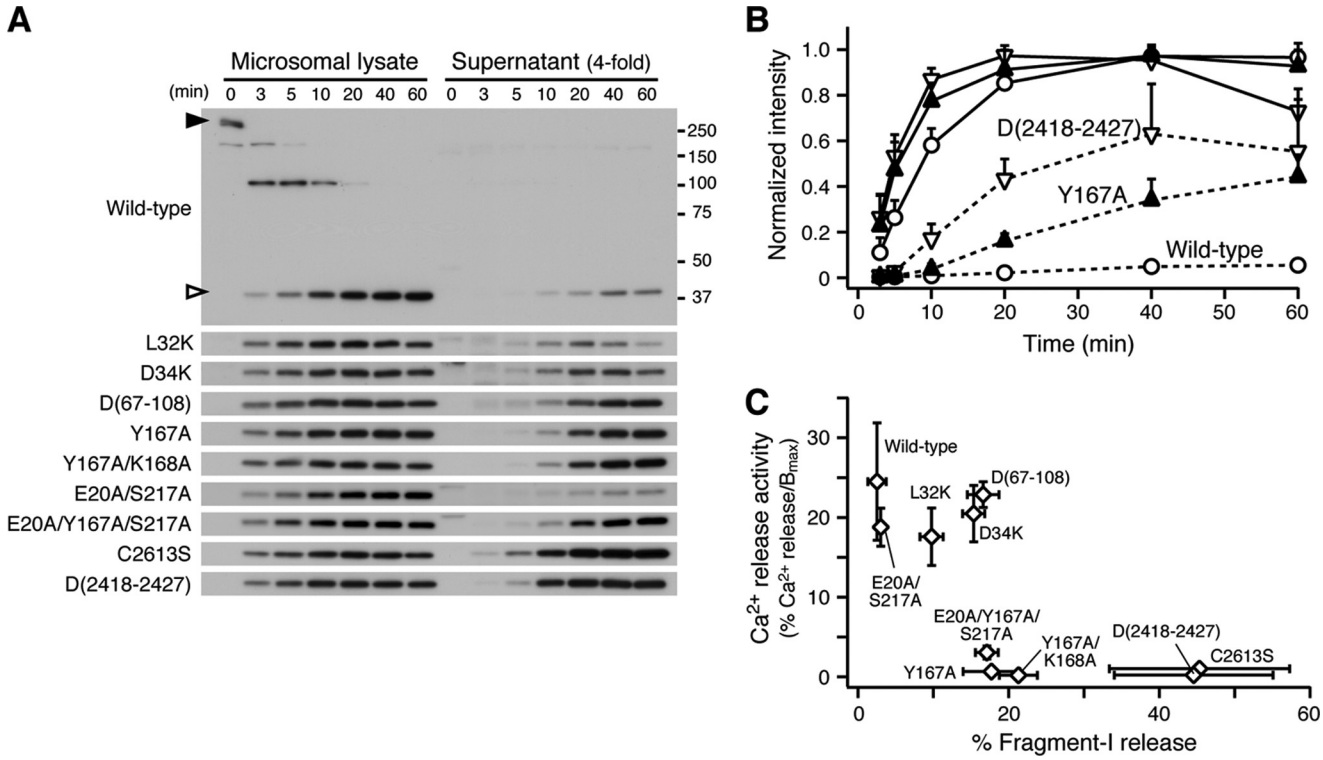

FIGURE 5. **Quantification of tryptic fragments dissociated from fragmented IP_3R1.** *A*, Western blot analysis of tryptic fragment I. Microsomal lysates treated with 2 μg/ml trypsin in the presence of 1 mM EGTA (total fragment I) and 4-fold concentrated supernatants (dissociated fragment I) were subjected to SDS-PAGE. Fragment I was detected with the N1 antibody (Fig. 1). Intact IP_3R1 (*filled arrowhead*) and the 40-kDa fragment I (*open arrowhead*) are indicated. Molecular size markers are shown on the *right* in kDa. Only the fragment I signals are shown for the mutants. *B*, temporal changes in the amounts of fragment I for wild-type IP_3R1 ($n = 10$), Y167A ($n = 8$), and D(2418–2427) ($n = 9$) in microsomal lysates (*continuous lines*) and supernatants (*broken lines*) during trypsin treatment in the presence of 1 mM EGTA. The intensities of signals detected in the 4-fold concentrated supernatants were divided by 4 and normalized by the maximal intensity detected in the microsomal lysates for each experiment. *C*, relationship between the fractions of tryptic fragment I in the supernatants and the Ca^{2+} release activities of the mutants. The amount of fragment I was quantified after 20 min of trypsin digestion in the presence of 1 mM EGTA. The Ca^{2+} release activity of each mutant is indicated as the fraction of Ca^{2+} release by the addition of 1 μM IP_3 divided by the expression level of the receptor (% Ca^{2+} *release*/B_{max}). The numbers of measurements of the Ca^{2+} release activity (n_1) and the fractions of fragment I (n_2) are shown in parentheses as (n_1/n_2): wild type (49/10), L32K (19/3), D34K (9/5), D(67–108) (16/3), Y167A (8/8), Y167A/K168A (8/4), E20A/S217A (6/4), E20A/Y167A/S217A (8/3), C2613S (7/3), and D(2418–2427) (6/9). *Error bars* in *B* and *C*, S.D.

As shown in our accompanying paper (57), the NMR and GST pull-down data suggested that Glu-20 and Ser-217 residues (Fig. 4*D*) are also involved in the interdomain interaction between N and C termini of IP_3R1. We therefore constructed E20A, S217A, and E20A/S217A mutants of mouse IP_3R1 and measured their IP_3-induced Ca^{2+} release activity using isolated microsomal vesicles. Neither single amino acid substitution at Glu-20 or Ser-217 (data not shown) nor simultaneous substitution of both sites (Fig. 4, *B* and *C*) changes the Ca^{2+} release activity of the channel. Interestingly, however, the E20A/Y167A/S217A mutant markedly regained the IP_3-induced Ca^{2+} release activity from the null activity of Y167A, resulting in ~10% of the wild-type channel activity (Fig. 4, *B* and *C*, and supplemental Fig. S6), suggesting that both Glu-20 and Ser-217 are also involved in the gating process of the channel.

Functional Roles of Tyr-167 in the Activation Gating of the IP_3R1 Channel—Using various mutants of the channel-forming domain of IP_3R1, Schug and Joseph (40) showed that there is an inverse correlation between the rate of IP_3-induced Ca^{2+} flux and the amount of tryptic fragment I of IP_3R1 dissociated from trypsin-treated microsomal vesicles. To investigate the functional roles of Tyr-167, we measured the amounts of tryptic fragment I recovered in supernatants during trypsin digestion (Fig. 5*A*). The total amount of fragment I of the wild-type channel in microsomal lysates reached its maximal value at 20 min and remained almost constant for at least 60 min (Fig. 5, *A* and *B*). Less than 10% of the fragment I generated in microsomal lysates was recovered in the supernatants after 60 min of digestion (Fig. 5*B*). As shown by Schug and Joseph (40), the D(2418–2427) mutant receptor lacking part of the M4-M5 linker (Fig. 1) exhibited enhanced release of fragment I, and ~40% of the fragment I was recovered in supernatants at 20 min (Fig. 5, *A* and *B*). The Y167A mutation resulted in an increase in the amount of fragment I in supernatants, but it was smaller than that of the D(2418–2427) mutant at both 20 and 40 min (Fig. 5*B*). Fig. 5*C* shows the relationship between the amounts of fragment I recovered in supernatants after 20 min of digestion and the Ca^{2+} release activities of the wild-type and mutant channels. The wild-type channel exhibited the minimum dissociation of fragment I (2.5 ± 1.2%) among the channels examined. The non-functional mutants, such as D(2418–2427), C2613S, Y167A, and Y167A/K168A, showed enhanced release of fragment I, but the amounts were varied from 18 ± 4% (Y167A) to 45 ± 12% (C2613S), depending on the mutation (Fig. 5*C*). The mutant channels with significant Ca^{2+} release activities, such as E20A/S217A, L32K, D34K, and D(67–108), showed relatively low release of fragment I (3.5 ± 0.5, 9.8 ± 1.5, 15 ± 1, and 17 ± 2%, respectively) (Fig. 5*C*). It is noteworthy that the rela-

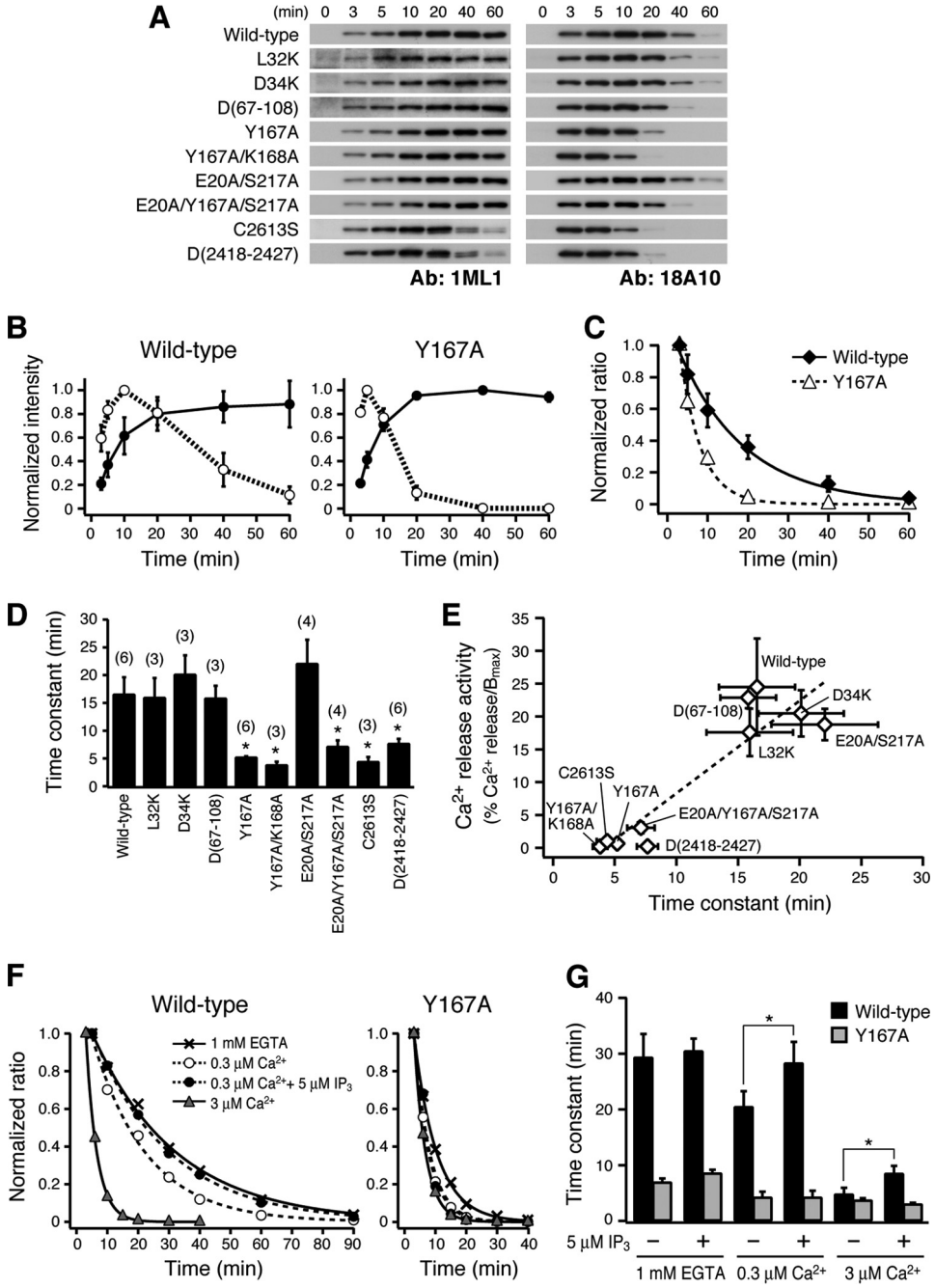

FIGURE 6. **Rapid degradation of tryptic fragment V of the mutants showing impaired IP_3-induced channel gating.** *A*, Western blot analysis of tryptic fragment V. Recombinant IP_3R1 channels were treated with 2 μg/ml trypsin in the presence of 1 mM EGTA. Tryptic fragment V (91 kDa) was detected with the 1ML1 (*left*) and 18A10 (*right*) antibodies. *B*, temporal changes in the fragment V signals detected with the 1ML1 (*filled circles*) and 18A10 (*open circles*) antibodies. The signals were normalized by the maximal intensity obtained for each measurement ($n = 6$). *C*, temporal changes in the amounts of 18A10-positive fragment V relative to the amounts of the 1ML1-positive fragment V. The ratios of the 18A10 signals to the 1ML1 signals were normalized by the ratio observed at the first sampling point (3 min), and the mean values from six independent measurements are shown. Data were fitted with a single-exponential function. *D*, time constants for the decreases in the relative amounts of 18A10-positive fragment V. The numbers of measurements are shown in *parentheses*. *, $p < 0.01$ *versus* the value of wild-type IP_3R1 by Scheffé's F-test. *E*, relationship between the time constants of tryptic fragment V degradation and the Ca^{2+} release activities of the mutant channels. The *broken line* indicates the result of a linear regression ($R^2 = 0.841$). *F*, effects of IP_3 and Ca^{2+} on the rates of decrease in the relative amounts of 18A10-positive fragment V. The temporal changes in the normalized ratios of the 18A10 signals to the 1ML1 signals are shown. *G*, time constants for the decreases in the relative amounts of 18A10-positive fragment V. The mean values from three measurements are shown. *, $p < 0.05$ by Student's *t* test. *Error bars* in *B–E* and *G*, S.D.

tive amounts of fragment I recovered in the supernatants were almost the same between the nonfunctional mutant Y167A and functional mutants, such as D34K and D(67–108) (Fig. 5*C*). These results indicate that the release of tryptic fragment I is not always correlated with the Ca^{2+} release activities of the channels.

In addition to the analyses of unliganded channels described above, we measured the effects of ligands, Ca^{2+} and IP_3, on the dissociation of the trypsinized fragments of IP_3R. The trypsin treatment was performed in the presence of 0.3 μM Ca^{2+}, 0.3 μM Ca^{2+} plus 5 μM IP_3, or 3 μM Ca^{2+}. The single channel open probability of IP_3R1 is dependent on the IP_3 concentration monotonically (45) and the Ca^{2+} concentration biphasically (19), and both ligands are required for channel opening (22). The second condition (0.3 μM Ca^{2+} plus 5 μM IP_3) is optimal for channel opening, whereas the channels are predominantly in the closed state under the other two conditions. The third condition (3 μM Ca^{2+}) may facilitate the transition of the channels to the Ca^{2+}-dependent inactivated state. As shown in supplemental Fig. S7*A*, the amounts of released fragment I of the wild-type channel and the mutants Y167A and D34K were not correlated with their Ca^{2+} release activities even in the presence of ligands. In wild-type IP_3R1, the release of the other three tryptic fragments (II, III, and IV; see Fig. 1) derived from the cytosolic region was small (~5%) and was not significantly changed regardless of the concentrations of ligands applied (supplemental Fig. S7*B*). We therefore concluded that IP_3R channel gating is not accompanied by gross changes in the interdomain interaction between the N-terminal cytosolic domain and the C-terminal channel-forming domain.

During the analyses of the tryptic fragments from various mutant IP_3R1 channels, we noted that the temporal patterns of Western blot signals of fragment V differed between the two anti-IP_3R1 antibodies, 1ML1 (26) and 18A10 (46),

which recognize different parts of the channel-forming domain (Fig. 1). As observed previously (37), the 1ML1 signals for the wild-type channel gradually increased during the trypsin treatment, whereas the 18A10 signals initially increased and then decreased (Fig. 6, *A* and *B*). Because the epitope for antibody 18A10 is located at the C-terminal end of the gatekeeper domain (residues 2736–2747) (47) and the electrophoretic mobility of the 1ML1 signals was not greatly changed even when the 18A10 signals had disappeared, a small C-terminal portion of the tryptic fragment V must be cleaved during the trypsin treatment. Similar temporal patterns were observed when the functional mutants L32K, D34K, D(67–108), and E20A/S217A were treated with trypsin (Fig. 6*A*). On the other hand, when the non-functional mutants, such as Y167A, Y167A/K168A, C2613S, and D(2418–2427), were treated with trypsin under the same conditions, the disappearance of the 18A10 signals was considerably accelerated (Fig. 6, *A* and *B*). In the case of C2613S and D(2418–2427), there is also progressive loss of the 1ML1 signal (Fig. 6*A*). To quantify the degradation rate of the 18A10-positive tryptic fragment V, we calculated the ratios of the intensities of the 18A10 signals and the 1ML1 signals. Because 1ML1 may react with fragment V regardless of its 18A10 reactivity, the calculated ratios correspond to the fractions of the 18A10-positive intact fragment V among the total amount of fragment V. As shown in Fig. 6*C*, the ratios decreased monotonically for wild-type IP_3R1 and the Y167A mutant with different time constants. Fig. 6*D* shows the mean time constants of the degradation rates in various mutant channels. The wild-type channel and the functional mutants L32K, D34K, D(67–108), and E20A/S217A showed longer time constants (>15 min), whereas the non-functional mutants Y167A, Y167A/K168A, C2613S, and D(2418–2427) had shorter time constants (<10 min). The time constant of the E20A/Y167A/S217A mutant, which showed a partial regain of Ca^{2+} release activity (Fig. 4*C*), was significantly longer than that of Y167A (7.1 ± 1.1 and 5.2 ± 0.2 min for E20A/Y167A/S217A and Y167A, respectively). The time constants exhibited a good correlation with the Ca^{2+} release activities of the mutant channels ($R^2 = 0.841$) (Fig. 6*E*). Therefore, the trypsin sensitivity of the C-terminal end of the gatekeeper domain has a marked correlation with the Ca^{2+} release activity of the channel.

To understand the relationships between the trypsin sensitivity of the gatekeeper domain and the functional states of the channel, we measured the effects of Ca^{2+} and IP_3 on the degradation rate of tryptic fragment V. In the absence of IP_3, the addition of Ca^{2+} accelerated the degradation of fragment V in a dose-dependent manner (Fig. 6, *F* and *G*). The addition of 5 μM IP_3 significantly increased the time constant in the presence of 0.3 μM and 3 μM Ca^{2+} (Fig. 6*G*). The rate of fragment V generation was not affected by the addition of the ligands (supplemental Fig. S8). Interestingly, the time constants of the Y167A mutant under all of the conditions examined were close to the time constant of the wild-type channel in the presence of 3 μM Ca^{2+} (Fig. 6, *F* and *G*). Although the issue of whether the structure of the Y167A mutant is identical to that of the wild-type channel in the presence of 3 μM Ca^{2+} is not clear, the results clearly showed that the structure of the gatekeeper domain of Y167A is different from that of the wild-type channel under the optimal conditions for channel opening (0.3 μM Ca^{2+} plus 5 μM IP_3).

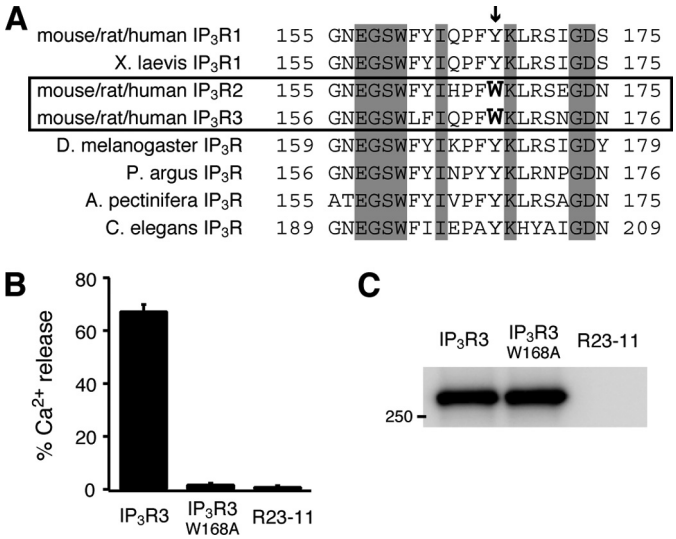

FIGURE 7. **Role of Trp-168 in IP_3R3.** *A*, alignment of the sequence around Tyr-167 in mouse IP_3R1 with other members of the IP_3R family. Identical residues are highlighted in *gray*. The NCBI accession numbers are X15373 (mouse IP_3R1), AB182288 (mouse IP_3R2), AB182289 (mouse IP_3R3), J05510 (rat IP_3R1), X61677 (rat IP_3R2), L06096 (rat IP_3R3), D26070 (human IP_3R1), D26350 (human IP_3R2), D26351 (human IP_3R3), D14400 (*X. laevis* IP_3R1), D90403 (*D. melanogaster* IP_3R), AF055079 (*P. argus* IP_3R), AB071372 (*A. pectinifera* IP_3R), and AJ243179 (*C. elegans* IP_3R). *B*, fractions of 10 μM IP_3-induced Ca^{2+} release from microsomal vesicles prepared from cells expressing wild-type IP_3R3 or IP_3R3_{W168A}, and from R23-11 cells ($n = 4$, 3, and 5, respectively). The total amount of releasable Ca^{2+} was measured by the addition of 2 μM 4-BrA23187. *Error bars*, S.D. *C*, Western blot analysis of microsomal fractions (4 μg of protein) prepared from cell lines expressing wild type or IP_3R3_{W168A} and from non-transfected R23-11 cells. IP_3R3 was detected with the KM1082 antibody (56). A molecular size marker is shown on the *left* in kDa.

Role of Trp-168 in IP_3R3 in the IP_3-induced Channel Opening—Tyr-167 in mouse IP_3R1 is conserved in the rat, human, and frog counterparts (Fig. 7*A*). The tyrosine residue is also conserved in IP_3Rs identified in invertebrates, such as the fly, lobster, starfish, and nematoda (Fig. 7*A*). However, tyrosine is replaced with tryptophan in mammalian IP_3R2 and IP_3R3 (Fig. 7*A*). To investigate the role of the tryptophan residue in the channel gating, we generated stable cell lines expressing an IP_3R3 mutant with Trp-168 substituted to alanine (IP_3R3_{W168A}) from IP_3R-deficient R23-11 cells. As shown in Fig. 7*B*, wild-type IP_3R3 mediated 67 ± 3% Ca^{2+} release from microsomal vesicles, whereas the IP_3R3_{W168A} mutant did not elicit measurable Ca^{2+} release even when the expression level of the mutant was similar to that of wild-type IP_3R3 (Fig. 7*C*). These results clearly demonstrate that Trp-168 is critical for the activation gating of IP_3R3.

DISCUSSION

The N-terminal ~220 amino acid residues of IP_3R form a bifunctional domain that is required for both IP_3 binding suppression (31) and IP_3-induced channel opening (30). In previous studies, we found that 7 conserved residues in the C1 region of this suppressor/coupling domain (Fig. 4*D*) are critical for the suppression of IP_3 binding (35) and that 11 non-conserved residues are responsible for the determination of isoform-specific IP_3 binding affinities (34). In this study, we identified amino

acid residues that are specifically required for channel gating within the suppressor/coupling domain. Among the 26 candidate residues for the possible site of the gating function, we found that simultaneous substitutions at both Tyr-167 and Lys-168 largely abolished the BCR-induced Ca^{2+} increase observed for the wild-type channel. When we measured IP_3-induced Ca^{2+} release from isolated microsomal vesicles, however, a single amino acid substitution at Tyr-167 was sufficient to completely abolish the IP_3-induced Ca^{2+} release activity, whereas a single substitution at Lys-168 resulted in an intermediate reduction in the Ca^{2+} release activity. The large reduction in the IP_3-induced Ca^{2+} flux from microsomal vesicles isolated from Y167A-expressing cells was not caused by Ca^{2+} leakage through Y167A channels because the rate of ATP-induced Ca^{2+} accumulation into vesicles was not significantly changed by exogenous expression of Y167A. The mutation at Tyr-167 did not hinder IP_3 binding to the receptor or normal folding of the molecule, suggesting that Tyr-167 is specifically required for the functional coupling between IP_3 binding and channel opening. It should be noted that, in the intact cells, substitution of IP_3R1 at either Tyr-167 or Lys-168 only exhibited small effects and that mutations of both residues were required for a profound effect on Ca^{2+} release. This property is not unique for IP_3R1 because substitution of Trp-168 in IP_3R3 was not sufficient to reduce BCR-induced Ca^{2+} release completely in intact cells, whereas Ca^{2+} release was not detected in the cells expressing W168A/K169A of IP_3R3 (supplemental Fig. S9). We do not know the reason for the discrepancy between the measurements using intact cells and microsomal vesicles, but these results suggest that there is some factor that influences the gating of IP_3R in cells. Further analyses of the residues near Tyr-167 and Lys-168 showed that substitution of Leu-169 induced an ~50% reduction in the Ca^{2+} release activity of the channel in isolated microsomal vesicles. Substitution at Glu-20 and Ser-217 partially rescued the impaired IP_3-induced Ca^{2+} release activity of the Y167A mutation in isolated microsomal vesicles. These data demonstrate that, although Tyr-167 plays the most critical role in the IP_3-induced gating function, Glu-20, Lys-168, Leu-169, and Ser-217 provide additional effects on the communication between the N-terminal ligand binding region and the C-terminal channel domain.

Functional Conservation of Tyr-167 in IP_3R1 and Trp-168 in IP_3R3 and Their Position in the Suppressor/Coupling Domain—Tyr-167 is conserved among vertebrate IP_3R1s and nonvertebrate IP_3Rs but is substituted with tryptophan in IP_3R2 and IP_3R3. In this study, we found that Trp-168 of mouse IP_3R3 was also critical for IP_3-induced channel opening. In our accompanying paper (57), the crystal structure of the suppressor/coupling domain of IP_3R3 was determined. The structure displays remarkable similarity with the previously reported structure of the IP_3R1 suppressor/coupling domain (35). In IP_3R1, Tyr-167 is located on the reverse side of the C1 region, in which the amino acid residues responsible for IP_3 binding suppression are clustered (Fig. 4*D*). Similarly, Trp-168 in IP_3R3 is situated on the same face of the structure on the reverse side of the C1 region. Glu-20, Lys-168, Leu-169, and Ser-217 of IP_3R1 are conserved in IP_3R2 and IP_3R3 (57) and are located adjacent to Tyr-167 on the surface of the domain (Fig. 4*D*). The functional conservation of the Tyr/Trp residue (Tyr-167 in IP_3R1 and Trp-168 in IP_3R3) strongly indicates that this position, together with neighboring residues, within the suppressor/coupling domain plays an important role in the mechanism by which the event of IP_3 binding at the N terminus of the receptor is transmitted to the channel at the C terminus.

Trp-168 in IP_3R3 is one of the 11 non-conserved residues identified as being critical for generating the IP_3R3-specific IP_3 binding affinity by attenuating the affinity of the IP_3-binding core (34). Similarly, the corresponding residue in IP_3R1 (Tyr-167) is responsible for determining the IP_3R1-specific affinity (34). The Y167A mutation actually increased the IP_3 binding affinity of IP_3R1 by ~2-fold. This is not because the Y167A mutation simply prevents a conformational transition of the IP_3-bound receptor toward channel opening, which should have resulted in a reduction of the apparent affinity (48). In fact, we confirmed that the Y167A mutation increases the IP_3 binding affinity even in the context of the N-terminal 604-amino acid construct $T604_{m1}$ (supplemental Table SIV). Therefore, the Tyr/Trp residue may have a bifunctional role to control both the degree of IP_3 binding suppression and the process of channel opening, whereas the IP_3 binding suppression itself is not essential for channel opening.

Functional Role of Tyr-167 in the Activation Gating of the IP_3R1 Channel—Why is Tyr-167 in the suppressor/coupling domain required for IP_3-induced channel opening? To probe the functionality of Tyr-167, we employed a previously reported proteolysis method that generates five stable tryptic fragments of the receptor that can self-assemble to form a functional channel (37). We found that the Y167A mutation facilitated the dissociation of tryptic fragment I, which contains the entire suppressor/coupling domain and part of the IP_3-binding core, from the assembly of fragmented IP_3R1, suggesting that Tyr-167 is involved in the intramolecular interaction of IP_3R1. Tyr-167 is not the sole residue responsible for the interaction between the N-terminal domain and the C-terminal domain because other mutants in which amino acid residues in the suppressor/coupling domain were altered, such as D34K and D(67–108), also released tryptic fragment I to similar extents as Y167A. Among the residues required for the interaction, Tyr-167 may play a vital role for channel gating because it directly forms the interface between these two domains. In our accompanying paper (57), we showed using NMR and GST pull-down assays that Tyr-167 directly interacted with the cytosolic M4-M5 linker in the C-terminal channel-forming domain. This interaction in IP_3R1 was preserved in IP_3R3, in which a similar interaction between Trp-168 and the M4-M5 linker was observed (57). We also identified residues Glu-19 and Ser-218 in IP_3R3 as interacting with the M4-M5 linker (57). The corresponding residues Glu-20 and Ser-217 in IP_3R1 were also critical for the interaction with the M4-M5 linker. In the present study, however, the mutations E20A and S217A of IP_3R1 did not change the dissociation rate of tryptic fragment I. When part of the M4-M5 linker was deleted, the dissociation rate was significantly faster than that of the Y167A mutant.

Therefore, other residues besides Glu-20, Tyr-167, and Ser-217 may also be involved in the interaction between the M4-M5 linker and N-terminal region.

In this study, one of the key roles of Tyr-167 for channel gating was identified during analyses of tryptic fragment V. The single amino acid substitution at Tyr-167 increased the rate of trypsin digestion of the C-terminal end of the gatekeeper domain. The non-functional mutants in which mutations were introduced within the C-terminal channel-forming domain, such as D(2418–2427) and C2613S, showed similar fast degradation rates of the gatekeeper domain, indicating that the trypsin sensitivity of the gatekeeper domain is directly correlated with the Ca^{2+} release activity of the channel. Interestingly, the gatekeeper domain of the wild-type channel was also rapidly digested with trypsin in the presence of 3 μM Ca^{2+}, whereas it was digested more slowly in the presence of lower concentrations of Ca^{2+}. IP_3 has much less effect on the degradation rate of the gatekeeper domain. Therefore, the transition between the high and low trypsin-sensitive states is a natural process that is controlled by the concentration of cytosolic Ca^{2+}. Under the optimal conditions for channel opening (0.3 μM Ca^{2+} plus 5 μM IP_3), the wild-type channel was in the low trypsin-sensitive state, whereas the Y167A mutant stayed in the high trypsin-sensitive state, as observed in the absence of Ca^{2+} and the presence of 3 μM Ca^{2+}. These data suggest that the single amino acid substitution at Tyr-167 can alter the conformational state of the C-terminal gatekeeper domain, thereby providing evidence for the significance of Tyr-167 in the functional coupling between the two termini of the channel. In other words, Tyr-167 functions to maintain the gatekeeper domain in a structure that is capable of opening when the channel binds IP_3 and Ca^{2+}.

The Mechanism Underlying the IP_3-induced Channel Opening—The identification of a critical residue within the suppressor/coupling domain and the analysis of the trypsin sensitivity of a single amino acid mutant of the identified residue revealed a possible role of the suppressor/coupling domain in the channel gating, in which Tyr-167 functions to control the C-terminal gatekeeper domain structure in both the resting and open states. Because there is no evidence that the gatekeeper domain directly interacts with the N-terminal IP_3-binding domain (40), we speculate that there is a three-way interaction among the N-terminal suppressor/coupling domain, the M4-M5 linker region, and the C-terminal gatekeeper domain (Fig. 8*A*, *left*), in which the Tyr/Trp contact region (Fig. 8*A*) plays a vital role in the proper communication among these components. The single amino acid substitution at the Tyr/Trp residue may disrupt the proper folding and/or accessibility of the gatekeeper domain by altering the three-way interaction (Fig. 8*A*, *right*).

A key question in the regulatory mechanism of IP_3R channels is how IP_3 binding triggers channel opening. The IP_3-binding core is composed of two stably folded structures, the β-trefoil II (βII) and Armadillo repeat-like α-helical fold (α) domains (33). The suppressor/coupling domain (structurally referred to as the β-trefoil I (βI) domain) (Fig. 8) has been shown to communicate with this IP_3-binding core to modulate the IP_3 binding affinity (31, 34). Chan *et al.* (49) showed that an isolated IP_3-binding construct (residues 1–604) containing the βI, βII, and α domains exists as a mixture of conformational substates containing compact and more extended structures and that IP_3 binding drives the conformational equilibrium toward more compact structures, which is consistent with our Förster resonance energy transfer study on the IP_3-binding region (15). If one speculates that the activation mechanism of IP_3R occurs in multiple steps, the data accumulated so far, including in the present study as well as in our accompanying paper (57), suggest the following scenario. First, binding of IP_3 to the ligand-binding core rearranges the domain-domain interaction and consequently the packing of the entire N-terminal region, including the βI, βII, and α domains. The signal originating from this local conformational change at the N terminus near the IP_3-binding region is likely to be transmitted to the channel domain through two possible routes: 1) direct communication from the suppressor/coupling domain to the M4-M5 linker in the channel domain through the Tyr/Trp contact region, for which the C-terminal gatekeeper domain also plays a role in the coupling mechanism (Fig. 8*B*, *left*) and/or 2) the central modulatory region, including residues 651–1130 (30) (Fig. 8*B*, *right*). These conformational changes may alter the Ca^{2+} sensitivity of the channel, which subsequently leads to full activation of the Ca^{2+} release function (50, 51). A single Ca^{2+} sensor site has been identified for the latter route (Fig. 1) (52), but the identification of all of the sites involved in the Ca^{2+}-dependent activation of the channel will be pivotal for understanding the

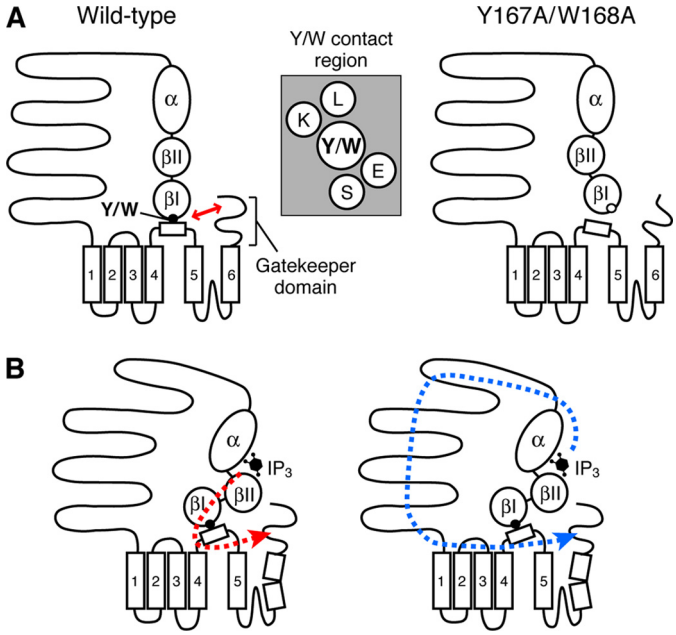

FIGURE 8. **Schematic models of the unliganded and liganded states of IP_3R.** *A*, a model for the unliganded state of IP_3R (*left*). Tyr-167 in IP_3R1 or Trp-168 in IP_3R3 (*Y/W*, *filled circle*) interacts with the M4-M5 linker and maintains the conformation of the gatekeeper domain in a low trypsin-sensitive form in the wild-type channel (*Wild-type*). The Tyr/Trp contact region is composed of Tyr-167/Trp-168 (*Y/W*) plus Glu-20/Glu19 (*E*), Lys-168/Lys-169 (*K*), Leu-169/Leu-170 (*L*), and Ser-217/Ser-218 (*S*) of IP_3R1/IP_3R3. Substitution of Tyr-167 or Trp-168 into alanine (*right*, *open circle*) disrupts the interaction with the M4-M5 linker, and the gatekeeper domain is maintained in a high trypsin-sensitive form (Y167A/W168A). *B*, a model for the liganded state of IP_3R. Two routes that relay IP_3 binding signals to the gatekeeper domain are shown by *red* and *blue arrows*. The gating hinge is assumed to be within the sixth membrane-spanning helix (30).

interplay between IP_3 and Ca^{2+} for the activation gating of IP_3R channels.

Acknowledgments—We thank Yoko Ueno and Kotomi Sawaguchi for excellent technical assistance. We thank Dr. Masahiro Enomoto for technical help in the construction of D(2418–2427) and for critical reading of the manuscript and Dr. Miwako Iwai for technical help. The hybridoma CaS/C1 developed by Dr. Douglas M. Fambrough was obtained from the Developmental Studies Hybridoma Bank developed under the auspices of the NICHD, National Institutes of Health, and maintained by the Department of Biology, University of Iowa (Iowa City, IA).

REFERENCES

1. Ferris, C. D., Huganir, R. L., Supattapone, S., and Snyder, S. H. (1989) *Nature* **342,** 87–89
2. Furuichi, T., Yoshikawa, S., Miyawaki, A., Wada, K., Maeda, N., and Mikoshiba, K. (1989) *Nature* **342,** 32–38
3. Miyawaki, A., Furuichi, T., Maeda, N., and Mikoshiba, K. (1990) *Neuron* **5,** 11–18
4. Miyazaki, S., Yuzaki, M., Nakada, K., Shirakawa, H., Nakanishi, S., Nakade, S., and Mikoshiba, K. (1992) *Science* **257,** 251–255
5. Muto, A., Kume, S., Inoue, T., Okano, H., and Mikoshiba, K. (1996) *J. Cell Biol.* **135,** 181–190
6. Kume, S., Muto, A., Inoue, T., Suga, K., Okano, H., and Mikoshiba, K. (1997) *Science* **278,** 1940–1943
7. Saneyoshi, T., Kume, S., Amasaki, Y., and Mikoshiba, K. (2002) *Nature* **417,** 295–299
8. Fukuda, N., Shirasu, M., Sato, K., Ebisui, E., Touhara, K., and Mikoshiba, K. (2008) *Eur. J. Neurosci.* **27,** 2665–2675
9. Futatsugi, A., Nakamura, T., Yamada, M. K., Ebisui, E., Nakamura, K., Uchida, K., Kitaguchi, T., Takahashi-Iwanaga, H., Noda, T., Aruga, J., and Mikoshiba, K. (2005) *Science* **309,** 2232–2234
10. Hisatsune, C., Yasumatsu, K., Takahashi-Iwanaga, H., Ogawa, N., Kuroda, Y., Yoshida, R., Ninomiya, Y., and Mikoshiba, K. (2007) *J. Biol. Chem.* **282,** 37225–37231
11. Matsumoto, M., Nakagawa, T., Inoue, T., Nagata, E., Tanaka, K., Takano, H., Minowa, O., Kuno, J., Sakakibara, S., Yamada, M., Yoneshima, H., Miyawaki, A., Fukuuchi, Y., Furuichi, T., Okano, H., Mikoshiba, K., and Noda, T. (1996) *Nature* **379,** 168–171
12. Inoue, T., Kato, K., Kohda, K., and Mikoshiba, K. (1998) *J. Neurosci.* **18,** 5366–5373
13. Nishiyama, M., Hong, K., Mikoshiba, K., Poo, M. M., and Kato, K. (2000) *Nature* **408,** 584–588
14. Akiyama, H., Matsu-ura, T., Mikoshiba, K., and Kamiguchi, H. (2009) *Sci. Signal.* **2,** ra34
15. Matsu-ura, T., Michikawa, T., Inoue, T., Miyawaki, A., Yoshida, M., and Mikoshiba, K. (2006) *J. Cell Biol.* **173,** 755–765
16. Furuichi, T., Kohda, K., Miyawaki, A., and Mikoshiba, K. (1994) *Curr. Opin Neurobiol.* **4,** 294–303
17. Iwai, M., Tateishi, Y., Hattori, M., Mizutani, A., Nakamura, T., Futatsugi, A., Inoue, T., Furuichi, T., Michikawa, T., and Mikoshiba, K. (2005) *J. Biol. Chem.* **280,** 10305–10317
18. Monkawa, T., Miyawaki, A., Sugiyama, T., Yoneshima, H., Yamamoto-Hino, M., Furuichi, T., Saruta, T., Hasegawa, M., and Mikoshiba, K. (1995) *J. Biol. Chem.* **270,** 14700–14704
19. Bezprozvanny, I., Watras, J., and Ehrlich, B. E. (1991) *Nature* **351,** 751–754
20. Iino, M. (1990) *J. Gen. Physiol.* **95,** 1103–1122
21. Tu, H., Wang, Z., and Bezprozvanny, I. (2005) *Biophys. J.* **88,** 1056–1069
22. Finch, E. A., Turner, T. J., and Goldin, S. M. (1991) *Science* **252,** 443–446
23. Mignery, G. A., and Südhof, T. C. (1990) *EMBO J.* **9,** 3893–3898
24. Miyawaki, A., Furuichi, T., Ryou, Y., Yoshikawa, S., Nakagawa, T., Saitoh, T., and Mikoshiba, K. (1991) *Proc. Natl. Acad. Sci. U.S.A.* **88,** 4911–4915
25. Galvan, D. L., Borrego-Diaz, E., Perez, P. J., and Mignery, G. A. (1999) *J. Biol. Chem.* **274,** 29483–29492
26. Michikawa, T., Hamanaka, H., Otsu, H., Yamamoto, A., Miyawaki, A., Furuichi, T., Tashiro, Y., and Mikoshiba, K. (1994) *J. Biol. Chem.* **269,** 9184–9189
27. Boehning, D., Mak, D. O., Foskett, J. K., and Joseph, S. K. (2001) *J. Biol. Chem.* **276,** 13509–13512
28. Shah, P. K., and Sowdhamini, R. (2001) *Protein Eng.* **14,** 867–874
29. Ramos-Franco, J., Galvan, D., Mignery, G. A., and Fill, M. (1999) *J. Gen. Physiol.* **114,** 243–250
30. Uchida, K., Miyauchi, H., Furuichi, T., Michikawa, T., and Mikoshiba, K. (2003) *J. Biol. Chem.* **278,** 16551–16560
31. Yoshikawa, F., Morita, M., Monkawa, T., Michikawa, T., Furuichi, T., and Mikoshiba, K. (1996) *J. Biol. Chem.* **271,** 18277–18284
32. Yoshikawa, F., Uchiyama, T., Iwasaki, H., Tomomori-Satoh, C., Tanaka, T., Furuichi, T., and Mikoshiba, K. (1999) *Biochem. Biophys. Res. Commun.* **257,** 792–797
33. Bosanac, I., Alattia, J. R., Mal, T. K., Chan, J., Talarico, S., Tong, F. K., Tong, K. I., Yoshikawa, F., Furuichi, T., Iwai, M., Michikawa, T., Mikoshiba, K., and Ikura, M. (2002) *Nature* **420,** 696–700
34. Iwai, M., Michikawa, T., Bosanac, I., Ikura, M., and Mikoshiba, K. (2007) *J. Biol. Chem.* **282,** 12755–12764
35. Bosanac, I., Yamazaki, H., Matsu-ura, T., Michikawa, T., Mikoshiba, K., and Ikura, M. (2005) *Mol. Cell* **17,** 193–203
36. Joseph, S. K., Pierson, S., and Samanta, S. (1995) *Biochem. J.* **307,** 859–865
37. Yoshikawa, F., Iwasaki, H., Michikawa, T., Furuichi, T., and Mikoshiba, K. (1999) *J. Biol. Chem.* **274,** 316–327
38. Nakayama, T., Hattori, M., Uchida, K., Nakamura, T., Tateishi, Y., Bannai, H., Iwai, M., Michikawa, T., Inoue, T., and Mikoshiba, K. (2004) *Biochem. J.* **377,** 299–307
39. Boehning, D., and Joseph, S. K. (2000) *EMBO J.* **19,** 5450–5459
40. Schug, Z. T., and Joseph, S. K. (2006) *J. Biol. Chem.* **281,** 24431–24440
41. Sugawara, H., Kurosaki, M., Takata, M., and Kurosaki, T. (1997) *EMBO J.* **16,** 3078–3088
42. Michikawa, T., Hirota, J., Kawano, S., Hiraoka, M., Yamada, M., Furuichi, T., and Mikoshiba, K. (1999) *Neuron* **23,** 799–808
43. Yoneshima, H., Miyawaki, A., Michikawa, T., Furuichi, T., and Mikoshiba, K. (1997) *Biochem. J.* **322,** 591–596
44. Grynkiewicz, G., Poenie, M., and Tsien, R. Y. (1985) *J. Biol. Chem.* **260,** 3440–3450
45. Watras, J., Bezprozvanny, I., and Ehrlich, B. E. (1991) *J. Neurosci.* **11,** 3239–3245
46. Maeda, N., Niinobe, M., and Mikoshiba, K. (1990) *EMBO J.* **9,** 61–67
47. Nakade, S., Maeda, N., and Mikoshiba, K. (1991) *Biochem. J.* **277,** 125–131
48. Colquhoun, D. (1998) *Br. J. Pharmacol.* **125,** 924–947
49. Chan, J., Whitten, A. E., Jeffries, C. M., Bosanac, I., Mal, T. K., Ito, J., Porumb, H., Michikawa, T., Mikoshiba, K., Trewhella, J., and Ikura, M. (2007) *J. Mol. Biol.* **373,** 1269–1280
50. Kaftan, E. J., Ehrlich, B. E., and Watras, J. (1997) *J. Gen. Physiol.* **110,** 529–538
51. Mak, D. O., McBride, S., and Foskett, J. K. (1998) *Proc. Natl. Acad. Sci. U.S.A.* **95,** 15821–15825
52. Miyakawa, T., Mizushima, A., Hirose, K., Yamazawa, T., Bezprozvanny, I., Kurosaki, T., and Iino, M. (2001) *EMBO J.* **20,** 1674–1680
53. Sienaert, I., De Smedt, H., Parys, J. B., Missiaen, L., Vanlingen, S., Sipma, H., and Casteels, R. (1996) *J. Biol. Chem.* **271,** 27005–27012
54. Sienaert, I., Missiaen, L., De Smedt, H., Parys, J. B., Sipma, H., and Casteels, R. (1997) *J. Biol. Chem.* **272,** 25899–25906
55. Yoshikawa, S., Tanimura, T., Miyawaki, A., Nakamura, M., Yuzaki, M., Furuichi, T., and Mikoshiba, K. (1992) *J. Biol. Chem.* **267,** 16613–16619
56. Sugiyama, T., Furuya, A., Monkawa, T., Yamamoto-Hino, M., Satoh, S., Ohmori, K., Miyawaki, A., Hanai, N., Mikoshiba, K., and Hasegawa, M. (1994) *FEBS Lett.* **354,** 149–154
57. Chan, J., Yamazaki, H., Ishiyama, N., Seo, M. D., Mal, T. K., Michikawa, T., Mikoshiba, K., and Ikura, M. (2010) *J. Biol. Chem.* **285,** 36092–36099